




Stability of the Néel quantum critical point in the presence of Dirac fermions

Huanzhi Hu ¹, Jennifer Lin,¹ Mikolaj D. Uryszek,¹ and Frank Krüger ^{1,2}

¹*London Centre for Nanotechnology, University College London, Gordon Street, London WC1H 0AH, United Kingdom*

²*ISIS Facility, Rutherford Appleton Laboratory, Chilton, Didcot, Oxfordshire OX11 0QX, United Kingdom*

 (Received 12 October 2022; revised 25 January 2023; accepted 31 January 2023; published 8 February 2023)

We investigate the stability of the Néel quantum critical point of two-dimensional quantum antiferromagnets, described by a nonlinear σ model, in the presence of a Kondo coupling to N_f flavors of two-component Dirac fermion fields. The long-wavelength order parameter fluctuations are subject to Landau damping by electronic particle-hole fluctuations. Using the momentum-shell renormalization group (RG), we demonstrate that the Landau damping is weakly irrelevant at the Néel quantum critical point, despite the fact that the corresponding self-energy correction dominates over the quadratic gradient terms in the IR limit. In the ordered phase, the Landau damping increases under the RG, indicative of damped spin-wave excitations. Although the Kondo coupling is weakly relevant, sufficiently strong Landau damping renders the Néel quantum critical point quasistable for $N_f \geq 4$ and thermodynamically stable for $N_f < 4$. In the latter case, we identify a multicritical point which describes the transition between the Néel critical and Kondo runaway regimes. The symmetry breaking at this fixed point results in the opening of a gap in the Dirac fermion spectrum. Approaching the multicritical point from the disordered phase, the fermionic quasiparticle residue vanishes, giving rise to non-Fermi-liquid behavior.

DOI: [10.1103/PhysRevB.107.085113](https://doi.org/10.1103/PhysRevB.107.085113)

I. INTRODUCTION

The discovery of topological insulators [1,2] has initiated an explosion of research into Dirac or Weyl semimetals and topological aspects of electronic band structures [3–6]. Dirac fermions with relativistic dispersion around pointlike Fermi surfaces can arise as low-energy excitations of weakly interacting electron systems. The most prominent example is graphene [7], which can be described by a tight-binding model of electrons on the half-filled honeycomb lattice.

Because of their pointlike Fermi surfaces nodal semimetals provide the simplest setting to study fermionic quantum criticality. While Dirac semimetals are stable against weak repulsive interactions, a consequence of the vanishing density of states at the Fermi level, sufficiently strong short-range interactions can give rise to a range of competing instabilities. For the extended Hubbard model on the half-filled honeycomb lattice rich phase diagrams were established [8–17], showing antiferromagnetic, charge ordered, Kekule, and topological Haldane phases. Sufficiently strong on-site Hubbard repulsion gives rise to a transition to an antiferromagnetic state with a gap in the electron spectrum that is proportional to the staggered magnetization.

Since the fermionic particle-hole excitations are gapless at such quantum phase transitions, the critical behavior falls outside the Landau-Ginzburg-Wilson paradigm of a pure order parameter description [18]. Instead, the nature of the transitions can be studied within a field theory that describes the coupling of the bosonic order parameter field, which is introduced through a Hubbard-Stratonovich decoupling of the interaction vertex, to the gapless Dirac fermions [19–21]. In the high-energy community, such field theories are known as

Gross-Neveu-Yukawa (GNY) theories [22,23]. For the antiferromagnetic transition driven by local Hubbard repulsion the staggered magnetization is described by an $O(3)$ order parameter field, and the field theory is usually referred to as the Heisenberg-GNY model. At the fermion-induced GNY fixed point, the fermions acquire an anomalous dimension, resulting in the fermion spectral functions with branch cuts rather than quasiparticle poles [20]. Such non-Fermi-liquid behavior is the hallmark of fermionic quantum criticality.

Interesting criticality is also expected if Dirac fermions are coupled to local magnetic moments. In the case of graphene, local moments can be introduced by adatoms [24] or defects [25], as evidenced by the experimental observation of a Kondo effect [26]. Moreover, the high Kondo temperatures [26] reflect the strong coupling between the local moments and the conduction electrons in Dirac materials [27]. In subsequent work [28] the unusual Kondo quantum criticality of magnetic adatoms in graphene and the very fast power-law decay of the Ruderman-Kittel-Kasuya-Yosida interaction between them were established.

In this paper we consider two-dimensional quantum antiferromagnets with Kondo coupling between the local moments and Dirac electrons. While two-dimensional Kondo lattice models with Dirac points close to the Fermi level might be rare, there is the prospect of engineering such models in heterostructures of graphene and two-dimensional van der Waals magnets [29], such as the honeycomb Heisenberg antiferromagnets MnPS₃ and NiPS₃ [30–36].

The aim of this work is to investigate the stability of the Néel quantum critical point of a local moment antiferromagnet against the Kondo coupling to Dirac fermions. We will demonstrate that the universal critical behavior of this model

is different from that of the Heisenberg-GNY theory which describes the antiferromagnetic ordering transition of a purely electronic model with local Hubbard repulsion between Dirac electrons.

The outline of this paper is as follows. In Sec. II we introduce the nonlinear σ model (NL σ M) describing the long-wavelength behavior of the two-dimensional quantum antiferromagnet with Kondo coupling to N_f Dirac fermion pairs. We discuss the importance of Landau damping of the Néel order parameter fluctuations by low-energy electronic particle-hole fluctuations. In Sec. III we analyze the Landau damped NL σ M. Using the momentum-shell renormalization group (RG), we demonstrate that Landau damping is weakly irrelevant at the Néel quantum critical point but increases in the ordered state, indicating that spin-wave excitations are damped. The full set of RG equations, including the Kondo coupling, are derived in Sec. IV and analyzed in Sec. V. We show that while the Kondo coupling is weakly relevant at the Néel quantum critical point, sufficiently strong Landau damping renders the critical point quasistable for any realistic system size for $N_f \geq 4$ and thermodynamically stable for $N_f < 4$. In the latter case, a multicritical point captures the transition between Néel critical and Kondo runaway regimes. We analyze the universal critical behavior associated with this fixed point. As demonstrated in Sec. VI, the behavior in $D = 3$ space-time dimensions is not accessible within an ϵ expansion above the lower critical dimension, $D = 2 + \epsilon$. Finally, in Sec. VII we summarize and discuss our results.

II. MODEL

Our starting model is a NL σ M which describes the Néel transition of a two-dimensional quantum antiferromagnet [37,38]. This model is coupled to N_f copies of two-component Dirac electrons via the conventional Kondo coupling. On a microscopic level this model could be realized in the low-energy limit of a quantum antiferromagnet on the honeycomb lattice with Kondo coupling to noninteracting electrons that move on either the same or adjacent honeycomb lattice at half filling. For this realization we would have $N_f = 4$ due to twofold spin and valley degeneracies. The effective continuum field theory at zero temperature is given by the imaginary-time path integral over the action $S = S_f + S_N + S_K$, with contributions

$$\begin{aligned} S_f &= \int_{\mathbf{q}, \omega} \bar{\psi}(\mathbf{q}, \omega) \left(-i \frac{\omega}{v_F} + q_x \tau_x + q_y \tau_y \right) \psi(\mathbf{q}, \omega), \\ S_N &= \frac{1}{2g} \int d^2 \mathbf{r} \int_0^\infty d\tau \left\{ (\nabla \vec{N})^2 + \frac{1}{c^2} (\partial_\tau \vec{N})^2 \right\}, \\ S_K &= \frac{\lambda}{\sqrt{N_f}} \int d^2 \mathbf{r} \int_0^\infty d\tau \bar{\psi}(\vec{N} \cdot \vec{\sigma} \otimes \tau_z) \psi, \end{aligned} \quad (1)$$

where S_f describes two-dimensional Dirac fermions with Fermi velocity v_F , written in terms of fermionic Grassmann fields ψ . The term S_N is the conventional NL σ M in terms of the staggered three-component Néel order parameter field $\vec{N}(\mathbf{r}, \tau)$, which satisfies the constraint $\vec{N}^2(\mathbf{r}, \tau) = 1$. Here c denotes the spin-wave velocity, and the coupling constant g is inversely proportional to the spin stiffness. The last contribution, S_K , is the Kondo coupling between the local moments

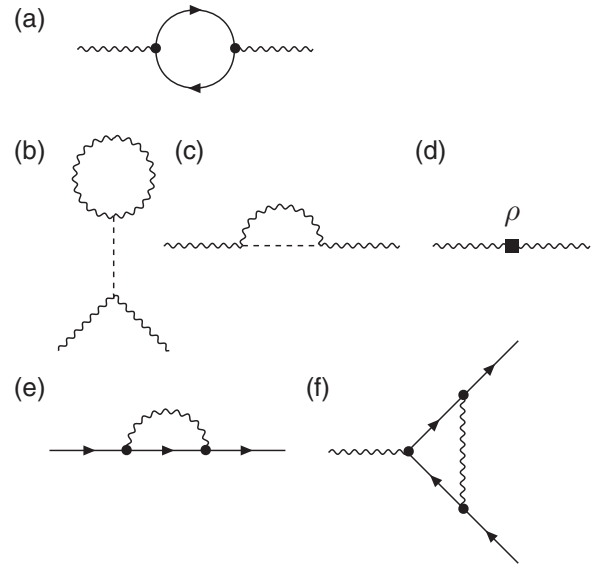


FIG. 1. One-loop diagrams relevant to our RG calculation. Solid lines represent fermionic degrees of freedom; wiggly lines represent the Néel order parameter fields. (a) The fermionic bubble diagram integrated over small momenta and frequencies gives rise to the nonanalytic Landau damping of long-wavelength order parameter fluctuations. The momentum-shell contribution of this diagram contributes to the renormalization of the coupling constant g of the NL σ M. (b)–(d) Diagrams relevant for the RG of the Landau damped NL σ M. The diagram in (b) is identical to zero, and (c) renormalizes the quadratic gradient terms and hence the coupling constant g . The unphysical mass term generated by (c) is canceled by the contribution in (d) from the functional integral measure. (e) The fermionic self-energy diagram renormalizes the overall prefactor of the free fermion action S_f . The scaling dimension of the fermion fields is determined such that the prefactor remains constant. (f) Diagram contributing to the renormalization of the Kondo coupling λ .

and Dirac electrons. Here $\vec{\sigma}$ is the vector of spin Pauli matrices, while the Pauli matrices τ_α act on sublattice space. Note that since \vec{N} describes the staggered magnetization the coupling has opposite signs on the two sublattices, resulting in the additional τ_z . The low-energy continuum field theory is subject to a UV momentum cutoff, $|\mathbf{q}| \leq \Lambda$.

As pointed out in the context of GNY theories [39,40], the Landau damping of the bosonic order parameter fluctuations by electronic particle-hole fluctuations gives rise to a self-energy contribution

$$\Pi(\mathbf{q}, \omega) = \gamma \sqrt{\mathbf{q}^2 + \omega^2/v_F^2} \quad (2)$$

to the inverse boson propagator in two spatial dimensions. This nonanalytic self-energy correction arises from the diagram in Fig. 1(a) from the integration of fermion modes near zero momenta and frequency. It is therefore not generated within the momentum-shell RG but needs to be included to correctly capture the universal critical behavior of GNY theories [39,40]. The form of the Landau damping does not depend on the number of order parameter components and is not affected by the fixed-length constraint of the Néel order parameter field. Note that although the bare Landau damping parameter γ_0 is determined by the square of the bare Kondo

coupling, $\gamma_0 \sim \lambda_0^2$, this relation is not preserved under the RG. We therefore treat γ and λ as independent coupling constants.

Under the RG there will be a nontrivial flow of the velocities c and v_F . For simplicity, we will focus on the case $v_F = c$, which is preserved under the RG. For convenience, we rescale to dimensionless momenta $\mathbf{k} = \mathbf{q}/\Lambda$ and frequencies $k_0 = \omega/(c\Lambda)$ and absorb the additional prefactors in a redefinition of the coupling constants. Since both the order parameter and fermion sectors are relativistic and frequency and momenta enter the zero-temperature field theory in the same way, the quantum critical behavior will be described by a dynamical exponent, $z = 1$. We will therefore treat frequency and momenta on equal footing and impose an isotropic cutoff in 2+1 dimensions, $\sqrt{\mathbf{k}^2 + k_0^2} \leq 1$. Note that the universal critical behavior is independent of the choice of the UV cutoff scheme.

III. LANDAU DAMPED NL σ M

We start by investigating the effects of Landau damping on the Néel transition in the case of vanishing Kondo coupling, $\lambda = 0$. Our starting point is the NL σ M

$$S_N = \frac{1}{2g} \int_k \Omega^{-1}(k) \vec{N}(k) \cdot \vec{N}(-k), \quad (3)$$

where we have defined $k = (\mathbf{k}, k_0)$ and $\int_k = \int \frac{d^3k_0}{2\pi} \int \frac{d^2\mathbf{k}}{(2\pi)^2}$, subject to the cutoff $|k| \leq 1$ for brevity, and include the Landau damping γ in the inverse propagator,

$$\Omega^{-1}(k) = k^2 + \gamma|k| = \mathbf{k}^2 + k_0^2 + \gamma\sqrt{\mathbf{k}^2 + k_0^2}. \quad (4)$$

We follow the conventional treatment [37,38,41] and decompose $\vec{N} = (\vec{\pi}, \sigma)$ and use the constraint $\sigma(\mathbf{r}, \tau) = \sqrt{1 - \vec{\pi}^2(\mathbf{r}, \tau)}$ to eliminate σ and derive an effective action in terms of the transverse fields $\vec{\pi}$. In the presence of Landau damping, we need to apply the constraint in momentum space, $\sigma(k) = \delta(k) - \frac{1}{2} \int_q \vec{\pi}(q) \vec{\pi}(k - q)$. This results in the effective action

$$\begin{aligned} S_N = & \frac{1}{2g} \int_k \Omega^{-1}(k) \vec{\pi}(k) \cdot \vec{\pi}(-k) - \frac{\rho}{2} \int_k \vec{\pi}(k) \cdot \vec{\pi}(-k) \\ & + \frac{1}{16g} \int_{k_1, \dots, k_4} \delta(k_1 + k_2 + k_3 + k_4) [\Omega^{-1}(k_1 + k_2) \\ & + \Omega^{-1}(k_3 + k_4)] [\vec{\pi}(k_1) \cdot \vec{\pi}(k_2)] [\vec{\pi}(k_3) \cdot \vec{\pi}(k_4)], \end{aligned} \quad (5)$$

where ρ is the density and the corresponding term arises from exponentiation and expansion of $1/[2\sqrt{1 - \vec{\pi}^2(\mathbf{r}, \tau)}]$ from the path-integral measure [41].

We integrate out modes with momenta and frequencies from an infinitesimal shell near the cutoff, $e^{-d\ell} \leq \sqrt{\mathbf{k}^2 + k_0^2} \leq 1$, followed by a rescaling of momenta, $\mathbf{k} \rightarrow \mathbf{k}e^{d\ell}$, and frequencies, $k_0 \rightarrow k_0 e^{z d\ell}$, with dynamical exponent $z = 1$. In addition, we rescale the transverse spin-fluctuation fields as $\vec{\pi}(k) \rightarrow \vec{\pi}(k) e^{-\Delta_\pi d\ell}$.

At one-loop order, the contraction of two order parameter fields,

$$(\pi_\alpha(k) \pi_\beta(k'))_0 = g \delta_{\alpha\beta} \delta(k + k') \Omega(k), \quad (6)$$

gives rise to the renormalization of the quadratic action by the quartic vertex. The diagram in Fig. 1(b) vanishes because

$\Omega^{-1}(0) = 0$. The diagram shown in Fig. 1(c) gives rise to a term $\sim k^2 \vec{\pi}(k) \cdot \vec{\pi}(-k)$ and hence a renormalization of the coupling constant g . In addition, it produces a mass term $\sim \vec{\pi}(k) \cdot \vec{\pi}(-k)$ which cancels exactly with the trivial term from the reduction of the density ρ by the shell contribution [Fig. 1(d)]. Evaluating the momentum-shell and frequency integrals and combining them with the rescaling contributions, we obtain the RG equations

$$\frac{d}{d\ell} \left(\frac{1}{2g} \right) = (-5 + 2\Delta_\pi) \frac{1}{2g} + \frac{1}{(2\pi)^2} \frac{1 + \gamma/3}{1 + \gamma}, \quad (7)$$

$$\frac{d}{d\ell} \left(\frac{\gamma}{2g} \right) = (-4 + 2\Delta_\pi) \frac{\gamma}{2g}. \quad (8)$$

The scaling dimension Δ_π of the transverse spin-fluctuation fields needs to be determined such that the constraint of the NL σ M is satisfied on all scales. This is the case only if the coupling constant g in front of the quartic vertex renormalizes in exactly the same way as the g in front of the quadratic action. Instead of evaluating the second-order, one-loop diagrams that renormalize the vertex, we employ a trick invented by Nelson and Pelcovits [41] to include a staggered magnetic field term, $-\frac{h}{2g} \int_{\mathbf{r}, \tau} \sigma(\mathbf{r}, \tau)$, in the action. Since the scaling of the magnetic field should not depend on the field direction and since the staggered magnetic field couples linearly to the Néel order parameter field, the scaling dimension of the applied field is equal to that of the order parameter field itself,

$$\frac{d}{d\ell} \left(\frac{h}{2g} \right) = \Delta_\pi \frac{h}{2g}. \quad (9)$$

On the other hand, we can use the constraint to expand $\sigma(\mathbf{r}, \tau)$ in terms of the $\vec{\pi}$ fields and explicitly compute the one-loop renormalization of the applied field,

$$\frac{d}{d\ell} \left(\frac{h}{2g} \right) = (-3 + 2\Delta_\pi) \frac{h}{2g} + \frac{1}{(2\pi)^2} \frac{h}{1 + \gamma}. \quad (10)$$

Equating Eqs. (9) and (10), we obtain

$$\Delta_\pi = 3 - \frac{2}{(2\pi)^2} \frac{g}{1 + \gamma}, \quad (11)$$

which results in the coupled RG equations

$$\frac{d\tilde{g}}{d\ell} = -\tilde{g} + \frac{1 - \gamma/3}{1 + \gamma} \tilde{g}^2, \quad (12)$$

$$\frac{d\gamma}{d\ell} = \gamma \left[1 - \frac{1 + \gamma/3}{1 + \gamma} \tilde{g} \right] \quad (13)$$

for $\tilde{g} = \frac{2}{(2\pi)^2} g$ and the Landau damping γ .

For $\gamma = 0$ we recover the RG equation of the conventional NL σ M in 2+1 space-time dimensions. This RG equation exhibits two fixed points: The attractive, Néel ordered fixed point at $\tilde{g} = 0$ and the critical fixed point at $\tilde{g} = \tilde{g}_c = 1$. For $\tilde{g}(0) < 1$ the RG flow is towards $\tilde{g} = 0$, corresponding to a freezing of transverse spin fluctuations on larger and larger scales. On the other hand, for $\tilde{g}(0) > 1$, $\tilde{g}(\ell) \rightarrow \infty$, corresponding to a vanishing of the spin stiffness and indicative of the destruction of long-range order by spatial and temporal fluctuations.

The coupled RG equations (12) and (13) do not exhibit any additional fixed points at finite γ . The RG flow in the

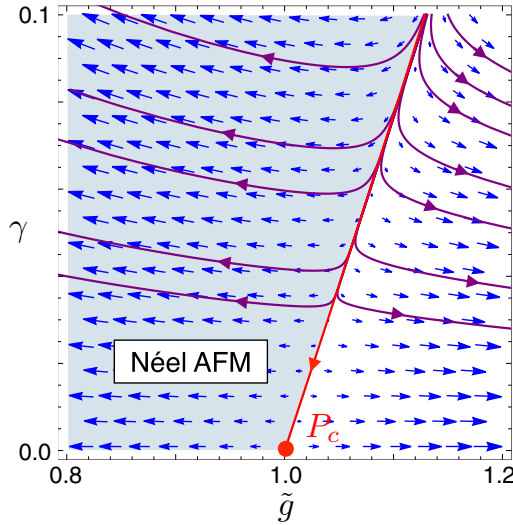


FIG. 2. RG flow of the Landau damped NL σ M as a function of the rescaled inverse spin stiffness $\tilde{g} = g/g_c$ and Landau damping γ . The red line separates the Néel antiferromagnet from the paramagnet. Along this separatrix, γ renormalizes to zero, demonstrating that the Néel quantum critical point P_c is stable against Landau damping. The increase of γ in the ordered phase indicates that spin-wave excitations are damped.

\tilde{g} - γ plane is shown in Fig. 2. In the antiferromagnetically ordered phase, $\gamma(\ell)$ increases, indicative of damped spin-wave excitations. At the critical fixed point of the Néel transition the Landau damping γ is weakly irrelevant. The separatrix between the Néel antiferromagnet and the quantum disordered phase is given by $\tilde{g} \approx 1 + \frac{4}{3}\gamma - \frac{4}{9}\gamma^2$. Along the separatrix and for an initial value $\gamma_0 = \gamma(0) \ll 1$, the Landau damping vanishes as $\gamma(\ell) = \gamma_0/(1 + \frac{2}{3}\gamma_0\ell)$.

IV. INCLUDING THE KONDO COUPLING TO DIRAC FERMIONS

We now include the Kondo coupling S_K between the order parameter field and N_f copies of two-component Dirac fermion fields, as given in Eq. (1). The momentum-shell contribution of the diagram in Fig. 1(a) will give rise to an additional correction to the NL σ M,

$$\delta S_N = -\frac{1}{2} \frac{\lambda^2}{N_f} \int_q^< \vec{N}(q) \cdot \vec{N}(-q) \times \int_k^> \text{Tr}\{\tau_z G_\psi(k) \tau_z G_\psi(k+q)\}, \quad (14)$$

where $\int_q^<$ and $\int_k^>$ denote frequency-momentum integrals over $|q| \leq e^{-d\ell}$ and $e^{-d\ell} \leq |k| \leq 1$, respectively. The fermionic Green's function in each of the N_f copies is given by

$$G_\psi(k) = \frac{ik_0 + k_x \tau_x + k_y \tau_y}{k_0^2 + \mathbf{k}^2}. \quad (15)$$

Note that the trace in Eq. (14) results in an additional factor of N_f . Expanding external momenta/frequencies $q = (\mathbf{q}, q_0)$

to quadratic order, we obtain

$$\delta S_N = -\frac{1}{3} \lambda^2 \frac{2}{(2\pi)^2} d\ell \int_q^< q^2 \vec{N}(q) \cdot \vec{N}(-q), \quad (16)$$

resulting in an additional contribution, $d(\frac{1}{2g}) = -\frac{1}{3} \lambda^2 \frac{2}{(2\pi)^2} d\ell$, to the renormalization of the coupling constant. This changes the RG equations for \tilde{g} and γ to

$$\frac{d\tilde{g}}{d\ell} = -\tilde{g} + \left[\frac{1-\gamma/3}{1+\gamma} + \frac{2}{3} \lambda^2 \right] \tilde{g}^2, \quad (17)$$

$$\frac{d\gamma}{d\ell} = \gamma \left[1 - \frac{1+\gamma/3}{1+\gamma} \tilde{g} + \frac{1}{3} \lambda^2 \tilde{g} \right]. \quad (18)$$

In order to determine the renormalization of the Kondo coupling constant λ , we first need to determine the scaling dimension Δ_ψ of the fermion fields. The diagram in Fig. 1(e) results in the correction

$$\begin{aligned} \delta S_f &= -\frac{2\lambda^2 g}{N_f} \int_k^< \bar{\psi}(k) \left(\int_q^> D(q) \tau_z G_\psi(k+q) \tau_z \right) \psi(k) \\ &= \frac{2}{3N_f} \frac{1}{1+\gamma} \lambda^2 \tilde{g} d\ell \int_k^< \bar{\psi}(k) G_\psi^{-1}(k) \psi(k), \end{aligned} \quad (19)$$

where the factor of 2 arises from the number of components of the transverse spin-fluctuation field $\vec{\pi}$, $N_\pi = 2$.

After rescaling frequency and momenta as before and fermion fields as $\psi(k) \rightarrow \psi(k) e^{-\Delta_\psi d\ell}$, we demand that the prefactor of S_f remain scale invariant, which results in

$$\Delta_\psi = 2 - \frac{1}{3N_f} \frac{1}{1+\gamma} \lambda^2 \tilde{g}. \quad (20)$$

The diagram that contributes to the renormalization of the Kondo vertex is shown in Fig. 1(f) and equals

$$\delta S_K = \frac{g\lambda^3}{\sqrt{N_f}^3} \sum_i \int_{k_1, k_2}^< \pi_i(k_1 - k_2) \bar{\psi}(k_1) \Omega_i \psi(k_2), \quad (21)$$

with coupling matrices

$$\begin{aligned} \Omega_i &= \sum_j \int_q^> D(q) (\sigma_j \otimes \tau_z) G_\psi(q) (\sigma_i \otimes \tau_z) \\ &\quad \times G_\psi(q) (\sigma_j \otimes \tau_z). \end{aligned} \quad (22)$$

Since G_ψ is independent of spin, we can evaluate the products of spin Pauli matrices and carry out the sum over j , $\sum_j \sigma_j \sigma_i \sigma_j = (2 - N_\pi) \sigma_i$. The momentum-shell integral is trivial, and we indeed find that Ω_i is proportional to the original Kondo coupling matrix $\sigma_i \otimes \tau_z$,

$$\Omega_i = \frac{2}{(2\pi)^2} (N_\pi - 2) \frac{1}{1+\gamma} d\ell (\sigma_i \otimes \tau_z). \quad (23)$$

However, the result crucially depends upon the number N_π of order parameter components, as discussed in the literature [42,43]. While the results for $N_\pi = 1$ and $N_\pi = 3$ are equal but of opposite sign, the diagram vanishes in the relevant case of $N_\pi = 2$ components, $\delta S_Y = 0$.

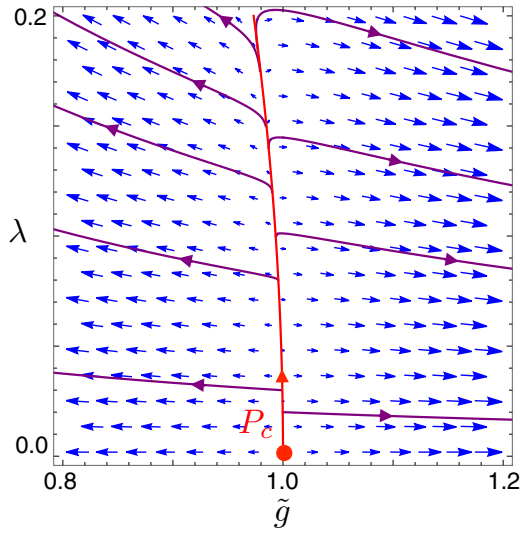


FIG. 3. RG flow as a function of inverse spin stiffness $\tilde{g} = g/g_c$ and Kondo coupling λ to Dirac fermions with $N_f = 4$ flavors. At the Néel quantum critical point P_c , the Kondo coupling is a weakly relevant perturbation, indicated by the increase of λ along the separatrix shown in red.

The rescaling of momenta, frequencies, and fields gives rise to the RG equation

$$\begin{aligned} \frac{d\lambda}{d\ell} &= (-6 + \Delta_\pi + 2\Delta_\psi)\lambda \\ &= \lambda \left[1 - \frac{\tilde{g}}{1 + \gamma} - \frac{2}{3N_f} \frac{\lambda^2 \tilde{g}}{1 + \gamma} \right] \end{aligned} \quad (24)$$

for the Kondo coupling λ .

V. ANALYSIS OF RG FLOW

We will now discuss the coupled RG equations for the inverse spin stiffness \tilde{g} (17), the Landau damping γ of the Néel order parameter (18), and the Kondo coupling λ to the Dirac fermions (24). In Sec. III we found that in the absence of Kondo coupling ($\lambda = 0$), the Landau damping γ is weakly irrelevant at the Néel quantum critical point P_c .

Let us first investigate the stability of P_c against Kondo coupling in the absence of Landau damping ($\gamma = 0$). In this case the RG equations reduce to $d\tilde{g}/d\ell = -\tilde{g} + (1 + \frac{2}{3}\lambda^2)\tilde{g}^2$ and $d\lambda/d\ell = \lambda(1 - \tilde{g} - \frac{2}{3N_f}\lambda^2\tilde{g})$. In this case we find a separatrix $\tilde{g} = 1 - \frac{2}{3}\lambda^2$, along which the flow of the Kondo coupling increases according to $d\lambda/d\ell = \frac{2}{3}(1 - 1/N_f)\lambda^3$, resulting in $\lambda(\ell) = \lambda_0/\sqrt{1 - \frac{4}{3}\lambda_0^2(1 - 1/N_f)\ell}$. The Néel quantum critical point is therefore very weakly unstable against the Kondo coupling to Dirac fermions. The RG flow in the \tilde{g} - λ plane is shown in Fig. 3.

To determine the critical surface in the three-dimensional parameter space of \tilde{g} , γ , and λ , we insert a polynomial ansatz $\tilde{g} = f(\gamma, \lambda)$ into the RG equations (17), (18), and (24). To second order we obtain

$$\tilde{g} = 1 + \frac{4}{3}\gamma - \frac{4}{9}\gamma^2 - \frac{2}{3}\lambda^2. \quad (25)$$

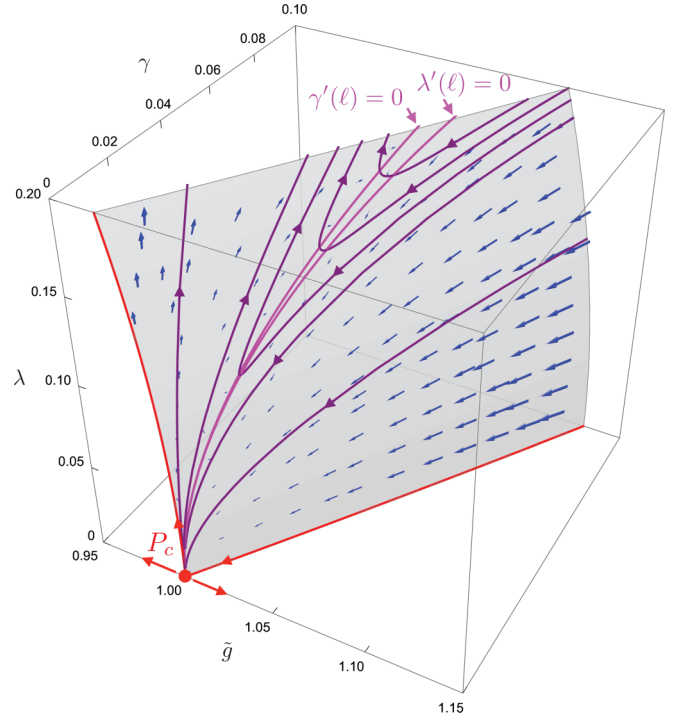


FIG. 4. RG flow within the critical surface for $N_f = 4$, relevant to Dirac electrons on the honeycomb lattice. The Néel quantum critical point P_c is stable against Landau damping γ but unstable against Kondo coupling λ . For sufficiently strong Landau damping, the RG flow is towards P_c until the trajectories turn to hit the magenta lines, which are given by $\gamma'(\ell) = 0$ and $\lambda'(\ell) = 0$ and closely track each other. At this point the RG flow becomes extremely slow, and the parameters acquire small metastable values.

The critical surface is shown in Fig. 4. As expected, the critical surface contains the separatrices in the $\lambda = 0$ and $\gamma = 0$ planes. For initial values of the coupling constants slightly outside the surface, the RG flow is away from the surface: The inverse spin stiffness \tilde{g} renormalizes to zero on one side, indicative of a freezing of spin-wave fluctuations, and to infinity on the other side, corresponding to a quantum disordered state. The Landau damping γ has a stabilizing effect on the Néel order, while the Kondo coupling λ has a destabilizing effect.

To analyze the competition between γ and λ within the critical surface we replace \tilde{g} in the corresponding RG equations, using Eq. (25),

$$\frac{d\gamma}{d\ell} = -\frac{2}{3}\gamma^2 + \frac{2}{3}\gamma^3 + \gamma\lambda^2, \quad (26)$$

$$\frac{d\lambda}{d\ell} = -\frac{1}{3}\gamma\lambda + \frac{7}{9}\gamma^2\lambda + \frac{2}{3}(1 - 1/N_f)\lambda^3, \quad (27)$$

where we have expanded up to cubic order in the coupling constants. For $N_f \geq 4$, the RG equations exhibit only a single fixed point at $\lambda = 0$ and $\gamma = 0$, corresponding to the Néel quantum critical point P_c . The RG flow in the critical surface and several trajectories obtained from numerical integration of the RG equations (26) and (27) are shown in Fig. 4 for the case with $N_f = 4$.

The RG flow is best understood in terms of the lines along which (i) $\gamma'(\ell) = 0$ and (ii) $\lambda'(\ell) = 0$, shown in magenta in Fig. 4 and given by (i) $\lambda^2 = \frac{2}{3}(\gamma - \gamma^2)$ and (ii) $\lambda^2 = \frac{1}{2(1-1/N_f)}(\gamma - \frac{7}{3}\gamma^2)$, respectively. These lines merge at P_c , and because they exhibit the same asymptotic functional form, $\lambda \sim \sqrt{\gamma}$, they closely track each other. As a result, the RG flow becomes very slow in the vicinity of this pair of lines, and it is not possible for trajectories to cross them on scales relevant to any realistic system size.

The case with $N_f = 4$, relevant to Dirac electrons on the honeycomb lattice, is the most extreme since in this case the coefficients of the leading $\sqrt{\gamma}$ terms are identical. For weak Landau damping, $\lambda^2 > \frac{2}{3}\gamma$, corresponding to points above the magenta lines, the flow is towards the regime of strong Kondo coupling. This indicates that the Néel quantum critical P_c point becomes unstable toward Kondo physics, which falls outside the validity of our analysis.

On the other hand, if the Landau damping is sufficiently strong, $\lambda^2 < \frac{2}{3}\gamma$, both $\lambda(\ell)$ and $\gamma(\ell)$ decrease under the RG. The corresponding trajectories approach P_c until they eventually turn to hit the magenta lines. Here the RG flow practically comes to a standstill, and $\lambda(\ell)$ and $\gamma(\ell)$ reach metastable plateau values γ_* and $\lambda_*^2 \approx \frac{2}{3}\gamma_*$. The nonzero Kondo coupling leads to the opening of a small electronic gap $\Delta \sim \lambda_* |\langle \tilde{N}(\mathbf{r}, \tau) \rangle|$ in the Néel ordered phase where the spin-rotational symmetry is broken. On the critical surface the finite values γ_* and λ_* result in an anomalous contribution to the scaling dimension Δ_ψ of the fermion fields, giving rise to non-Fermi-liquid behavior. However, the corresponding critical exponents are nonuniversal since the behavior is not associated with a true fixed point.

For $N_f < 4$ the RG equations (26) and (27) exhibit an additional fixed point \tilde{P}_c at

$$\tilde{\gamma}_c = \frac{4 - N_f}{4 + 3N_f}, \quad \tilde{\lambda}_c^2 = \frac{8 N_f (4 - N_f)}{3 (4 + 3N_f)^2}, \quad (28)$$

which merges with the Néel quantum critical point P_c as $N_f \rightarrow 4$, showing again that the case with $N_f = 4$ is marginal.

In Fig. 5 the RG flow of γ and λ within the critical surface is shown for the representative case with $N_f = 2$. In the blue region the RG flow is towards P_c , demonstrating that the Néel fixed point is thermodynamically stable rather than metastable. In the regime of small Kondo coupling λ , this stability is achieved by finite, but very small, Landau damping γ . In the purple region the RG flow is towards large values of γ and λ , beyond the validity of our RG equations. The transition between this Kondo runaway regime and the Néel critical region is described by the multicritical fixed point \tilde{P}_c .

We proceed to analyze the universal critical behavior of the multicritical point \tilde{P}_c for general $N_f < 4$. The correlation length exponent $\tilde{\nu}$ can be obtained from linearizing the RG equation for the inverse spin stiffness (17) around the critical value $\tilde{g}_c \approx 1 + \frac{4}{3}\tilde{\gamma}_c - \frac{2}{3}\tilde{\lambda}_c^2$. The resulting RG equation is of the general form $d(\tilde{g} - \tilde{g}_c)/d\ell = \tilde{\nu}^{-1}(\tilde{g} - \tilde{g}_c)$. A short calculation gives $\tilde{\nu} = 1$, which is identical to the correlation length exponent $\nu = 1$ at the Néel quantum critical point P_c .

From the scaling dimension Δ_π (11) of the transverse spin fluctuations fields $\tilde{\pi}$ we obtain the anomalous dimension $\tilde{\eta}_\pi =$

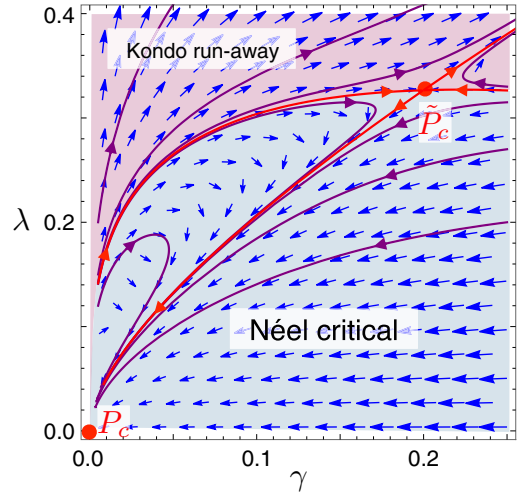


FIG. 5. RG flow of the Landau damping γ and the Kondo coupling λ within the critical surface for $N_f = 2$. The Néel quantum critical point P_c is thermodynamically stable in the blue region. In the purple region the flow is towards increasing λ , indicative of strong-coupling Kondo physics. The transition between the two regimes is controlled by a new multicritical point \tilde{P}_c .

1 at the Néel critical point P_c and

$$\tilde{\eta}_\pi = \frac{\tilde{g}_c}{1 + \tilde{\gamma}_c} \approx 1 + \frac{1}{9} \frac{(4 - N_f)(12 - 7N_f)}{(4 + 3N_f)^2} \quad (29)$$

at the multicritical point \tilde{P}_c . The additional contribution to $\tilde{\eta}_\pi$ results in a slightly different exponent of the algebraic order parameter correlations at criticality, $\langle \tilde{\pi}(\mathbf{r}) \tilde{\pi}(\mathbf{0}) \rangle \sim r^{-D+2-\tilde{\eta}_\pi}$, and corrections to other critical exponents, which can be obtained from the conventional scaling and hyperscaling relations.

Due to the finite value $\tilde{\lambda}_c$ (28) of the Kondo coupling at \tilde{P}_c , the symmetry breaking transition will be accompanied by the opening of a gap [20],

$$\Delta \sim (\tilde{g}_c - \tilde{g})^{z\tilde{\nu}} = (\tilde{g}_c - \tilde{g}), \quad (30)$$

in the Dirac fermion spectrum for $\tilde{g} < \tilde{g}_c$ in the Néel ordered phase. Moreover, at \tilde{P}_c the fermions acquire a small anomalous dimension [see Eq. (20)],

$$\tilde{\eta}_\psi = \frac{1}{3N_f} \frac{\tilde{\lambda}_c^2 \tilde{g}_c}{1 + \tilde{\gamma}_c} \approx \frac{8}{9} \frac{4 - N_f}{(4 + 3N_f)^2}, \quad (31)$$

which implies that the fermion Green's function has branch cuts rather than quasiparticle poles. The multicritical point \tilde{P}_c is therefore associated with non-Fermi-liquid behavior. From a scaling analysis of the fermionic spectral function [20] we find that the quasiparticle pole strength vanishes as

$$Z \sim (\tilde{g} - \tilde{g}_c)^{(z-1+\tilde{\eta}_\psi)\tilde{\nu}} = (\tilde{g} - \tilde{g}_c)^{\tilde{\eta}_\psi} \quad (32)$$

as the critical point is approached from the semimetallic, nonmagnetic phase ($\tilde{g} > \tilde{g}_c$).

VI. COMPARISON WITH THE ϵ EXPANSION

We now address the question of whether the same qualitative behavior can be found within an ϵ expansion above the

lower critical dimension, $D = 2 + \epsilon$. Although such an expansion gives analytic control of the criticality of the NL σ M [41,44], the Padé-Borel extrapolation to $\epsilon = 1$ may be problematic due to a lack of sign oscillations in the coefficients of the ϵ expansion of $1/\nu$ [45].

An additional problem arises when the NL σ M is coupled to Dirac fermions since the form of the resulting Landau damping of the Néel order parameter field explicitly depends on the dimension D , $\Pi(\mathbf{k}) = \gamma|\mathbf{k}|^{D-2}$ [40]. At one-loop order the RG equations for the inverse spin stiffness $\tilde{g} = g/(2\pi)$ and the Landau damping γ in $D = 2 + \epsilon$ are given by

$$\frac{d\tilde{g}}{d\ell} = -\epsilon\tilde{g} + \frac{1 - \gamma\epsilon^2/4}{1 + \gamma}\tilde{g}^2, \quad (33)$$

$$\frac{d\gamma}{d\ell} = \gamma\left[2 - \epsilon - \frac{1 + \gamma\epsilon^2/4}{1 + \gamma}\tilde{g}\right], \quad (34)$$

where we have determined the scaling dimension of the order parameter field $\Delta_\pi = 2 + \epsilon - \tilde{g}/(1 + \gamma)$ from the renormalization of an auxiliary magnetic field, as before.

Without Landau damping, $\gamma = 0$, we obtain the Néel quantum critical point at $\tilde{g}_c = \epsilon$. At the critical spin stiffness the linearized RG equation for γ is equal to $d\gamma/d\ell = 2(1 - \epsilon)\gamma$, showing that near the lower critical dimension the Landau damping is a relevant perturbation.

Interestingly, the shell contribution of the diagram in Fig. 1(a) is equal to zero in $D = 2$ due to a vanishing angular integral. As a result, the Kondo coupling λ does not contribute to the renormalization of \tilde{g} and γ , unlike in $D = 3$.

For similar reasons, the angular integration over the ($D = 2$)-dimensional shell causes the fermionic self-energy diagram, shown in Fig. 1(e), to vanish. The fermion field therefore does not acquire an anomalous dimension, and the scaling dimension is trivial, $\Delta_\psi = (3 + \epsilon)/2$. From the scaling dimensions Δ_π and Δ_ψ we obtain the renormalization of the Kondo coupling,

$$\frac{d\lambda}{d\ell} = \lambda\left[1 - \frac{\tilde{g}}{1 + \gamma}\right]. \quad (35)$$

At $\tilde{g}_c = \epsilon$ and $\gamma = 0$ the RG equation reduces to $d\lambda/d\ell = (1 - \epsilon)\lambda$, demonstrating that the Kondo coupling is a relevant perturbation at the Néel quantum critical point for $\epsilon < 1$. Note that for $\epsilon = 1$ both the Landau damping γ and the Kondo coupling λ become marginal, consistent with our calculation in $D = 3$.

VII. DISCUSSION

We have investigated the stability of the Néel quantum critical point of a two-dimensional quantum antiferromagnet with a Kondo coupling to N_f flavors of two-component Dirac fermion fields. For $N_f = 4$ this would describe Dirac electrons on the honeycomb lattice with twofold spin and valley degeneracies.

The resulting long-wavelength field theory is given by a NL σ M coupled to the Dirac fermion fields. It is crucial to account for the Landau damping of the Néel order parameter field. From simple scaling arguments, the resulting self-energy correction to the order parameter propagator is expected to dominate the IR physics.

At first glance the field theory seems very similar to the Heisenberg-GNY theory, which describes the criticality in a purely electronic model with strong local repulsions between the Dirac electrons. There are crucial differences, however. While in the GNY theory the quantum phase transition is tuned by the mass of the order parameter field, the NL σ M contains only gradient terms, and the criticality occurs as a function of the inverse spin stiffness. It is therefore essential to follow the scale dependence of the order parameter propagator with both the quadratic gradient terms and the nonanalytic self-energy correction from Landau damping. In the Heisenberg-GNY theory, on the other hand, the quadratic gradient terms can be discarded.

Another important difference is that the scaling dimension of the transverse spin-fluctuation field of the NL σ M is fixed by the requirement that the constraint $\vec{N}^2 = 1$ is satisfied on all length scales. As a result, the boson scaling dimension cannot be used to enforce scale invariance of the Kondo coupling, in contrast to the large- N_f Heisenberg-GNY theory.

We have employed momentum-shell RG to analyze the scale dependence of the inverse spin stiffness g , the Landau damping γ , and the Kondo coupling λ . Although γ and λ are initially linked to each other via the fermionic polarization diagram, the two parameters flow independently under the RG. At the Néel quantum critical point the scaling dimensions of both γ and λ vanish, and a bifurcation analysis is required. We have investigated the coupled RG flow of the two perturbations within the critical surface $g = f(\gamma, \lambda)$, which contains the unperturbed Néel quantum critical point and separates the regions where transverse spin fluctuations freeze or diverge.

The flow within the critical surface shows that while the Landau damping γ is weakly irrelevant at the Néel critical point, the Kondo coupling λ is a weakly relevant perturbation. Interestingly, the interplay between the two parameters crucially depends on the number N_f of Dirac fermion flavors. For $N_f \geq 4$, sufficiently strong Landau damping renders the Néel quantum critical point metastable. This is evident from an RG flow towards the Néel critical point up to scales larger than those relevant to experiments. This behavior is most pronounced for the marginal case $N_f = 4$, representing Dirac electrons on the honeycomb lattice.

For $N_f < 4$ the Néel critical point becomes thermodynamically stable over a region where the Landau damping dominates over the Kondo coupling. We have established a multicritical point on the critical surface which controls the transition between the Néel critical and Kondo runaway regimes. The finite values of γ and λ lead to distinct critical exponents and an anomalous dimension of the fermion fields, resulting in non-Fermi-liquid behavior. It would be interesting to investigate whether our results are robust at higher-loop order and whether the change in behavior still occurs at $N_f = 4$ or at a different number of Dirac fermion flavors.

Finally, we have investigated the problem in $D = 2 + \epsilon$ space-time dimensions where the RG calculation of the NL σ M is controlled. We found that near the lower critical dimension both the Landau damping and the Kondo coupling are relevant perturbations at the Néel quantum critical point, resulting in a runaway flow. Unfortunately, the rich behavior in 2+1 dimensions is not accessible within an ϵ expansion above the lower critical dimension, and the large- N_f limit does

not provide analytic control as in the Heisenberg-GNY theory. Nevertheless, our results point towards interesting novel

critical behavior that could potentially be further investigated using quantum Monte Carlo.

-
- [1] M. Z. Hasan and C. L. Kane, *Rev. Mod. Phys.* **82**, 3045 (2010).
- [2] X.-L. Qi and S.-C. Zhang, *Rev. Mod. Phys.* **83**, 1057 (2011).
- [3] O. Vafek and A. Vishwanath, *Annu. Rev. Condens. Matter Phys.* **5**, 83 (2014).
- [4] B. Yan and C. Felser, *Annu. Rev. Condens. Matter Phys.* **8**, 337 (2017).
- [5] N. P. Armitage, E. J. Mele, and A. Vishwanath, *Rev. Mod. Phys.* **90**, 015001 (2018).
- [6] M. Z. Hasan, G. Chang, I. Belopolski, G. Bian, S.-Y. Xu, and J.-X. Yin, *Nat. Rev. Mater.* **6**, 784 (2021).
- [7] A. H. Castro Neto, F. Guinea, N. M. R. Peres, K. S. Novoselov, and A. K. Geim, *Rev. Mod. Phys.* **81**, 109 (2009).
- [8] A. G. Grushin, E. V. Castro, A. Cortijo, F. de Juan, M. A. H. Vozmediano, and B. Valenzuela, *Phys. Rev. B* **87**, 085136 (2013).
- [9] N. A. García-Martínez, A. G. Grushin, T. Neupert, B. Valenzuela, and E. V. Castro, *Phys. Rev. B* **88**, 245123 (2013).
- [10] M. Daghofer and M. Hohenadler, *Phys. Rev. B* **89**, 035103 (2014).
- [11] S. Capponi and A. M. Läuchli, *Phys. Rev. B* **92**, 085146 (2015).
- [12] J. Motruk, A. G. Grushin, F. de Juan, and F. Pollmann, *Phys. Rev. B* **92**, 085147 (2015).
- [13] D. D. Scherer, M. M. Scherer, and C. Honerkamp, *Phys. Rev. B* **92**, 155137 (2015).
- [14] Y. Volpez, D. D. Scherer, and M. M. Scherer, *Phys. Rev. B* **94**, 165107 (2016).
- [15] M. Kurita, Y. Yamaji, and M. Imada, *Phys. Rev. B* **94**, 125131 (2016).
- [16] D. S. de la Peña, J. Lichtenstein, and C. Honerkamp, *Phys. Rev. B* **95**, 085143 (2017).
- [17] E. Christou, B. Uchoa, and F. Krüger, *Phys. Rev. B* **98**, 161120(R) (2018).
- [18] Z.-X. Li, Y.-F. Jiang, S.-K. Jian, and H. Yao, *Nat. Commun.* **8**, 314 (2017).
- [19] I. F. Herbut, *Phys. Rev. Lett.* **97**, 146401 (2006).
- [20] I. F. Herbut, V. Juricic, and B. Roy, *Phys. Rev. B* **79**, 085116 (2009).
- [21] F. F. Assaad and I. F. Herbut, *Phys. Rev. X* **3**, 031010 (2013).
- [22] D. J. Gross and A. Neveu, *Phys. Rev. D* **10**, 3235 (1974).
- [23] J. Zinn-Justin, *Nucl. Phys. B* **367**, 105 (1991).
- [24] P. O. Lehtinen, A. S. Foster, A. Ayuela, A. Krasheninnikov, K. Nordlund, and R. M. Nieminen, *Phys. Rev. Lett.* **91**, 017202 (2003).
- [25] J.-H. Chen, W. G. Cullen, C. Jang, M. S. Fuhrer, and E. D. Williams, *Phys. Rev. Lett.* **102**, 236805 (2009).
- [26] J.-H. Chen, L. Li, W. G. Cullen, E. D. Williams, and M. S. Fuhrer, *Nat. Phys.* **7**, 535 (2011).
- [27] M. Hentschel and F. Guinea, *Phys. Rev. B* **76**, 115407 (2007).
- [28] B. Uchoa, T. G. Rappoport, and A. H. Castro Neto, *Phys. Rev. Lett.* **106**, 016801 (2011).
- [29] K. S. Burch, D. Mandrus, and J.-G. Park, *Nature (London)* **563**, 47 (2018).
- [30] P. A. Joy and S. Vasudevan, *Phys. Rev. B* **46**, 5425 (1992).
- [31] N. Chandrasekharan and S. Vasudevan, *J. Phys.: Condens. Matter* **6**, 4569 (1994).
- [32] A. R. Wildes, B. Roessli, B. Lebeck, and K. W. Godfrey, *J. Phys.: Condens. Matter* **10**, 6417 (1998).
- [33] A. R. Wildes, H. M. Rønnow, B. Roessli, M. J. Harris, and K. W. Godfrey, *Phys. Rev. B* **74**, 094422 (2006).
- [34] A. R. Wildes, V. Simonet, E. Ressouche, G. J. McIntyre, M. Avdeev, E. Suard, S. A. J. Kimber, D. Lançon, G. Pepe, B. Moubaraki, and T. J. Hicks, *Phys. Rev. B* **92**, 224408 (2015).
- [35] D. Lançon, R. A. Ewings, T. Guidi, F. Formisano, and A. R. Wildes, *Phys. Rev. B* **98**, 134414 (2018).
- [36] K. Kim, S. Y. Lim, J. Kim, J.-U. Lee, S. Lee, P. Kim, K. Park, S. Son, C.-H. Park, J.-G. Park, and H. Cheong, *2D Mater.* **6**, 041001 (2019).
- [37] S. Chakravarty, B. I. Halperin, and D. R. Nelson, *Phys. Rev. Lett.* **60**, 1057 (1988).
- [38] S. Chakravarty, B. I. Halperin, and D. R. Nelson, *Phys. Rev. B* **39**, 2344 (1989).
- [39] H. Isobe, B.-J. Yang, A. Chubukov, J. Schmalian, and N. Nagaosa, *Phys. Rev. Lett.* **116**, 076803 (2016).
- [40] M. D. Uryszek, F. Krüger, and E. Christou, *Phys. Rev. Res.* **2**, 043265 (2020).
- [41] D. R. Nelson and R. A. Pelcovits, *Phys. Rev. B* **16**, 2191 (1977).
- [42] S. Sur and B. Roy, *Phys. Rev. Lett.* **123**, 207601 (2019).
- [43] M. D. Uryszek, E. Christou, A. Jaefari, F. Krüger, and B. Uchoa, *Phys. Rev. B* **100**, 155101 (2019).
- [44] A. Polyakov, *Phys. Lett. B* **59**, 79 (1975).
- [45] S. Hikami and E. Brezin, *J. Phys. A*: **11**, 1141 (1978).